

Contribution of X-ray CMT image processing to the modelling of pyrocarbon Chemical Vapour Infiltration

G. L. Vignoles^{1*}, C. Mulat^{1,2}, C. Germain^{1,3}, O. Coindreau¹, S. Delettrez¹, G. Chollon⁴

¹ University Bordeaux 1, Lab for ThermoStructural Composites (LCTS), CNRS UMR 5801, 3, Allée La Boétie, Pessac, F33600 (France)

² University Bordeaux 1, Lab for Integration from Materials to Structures (IMS), CNRS UMR 5218, 351 Cours de la Libération, F-33405 Talence Cedex (France)

³ ENITAB, Lab for Integration from Materials to Structures (IMS), CNRS UMR 5218, 351 Cours de la Libération, F-33405 Talence Cedex (France)

⁴ CNRS, Lab for ThermoStructural Composites (LCTS), CNRS UMR 5801, 3, Allée La Boétie, Pessac, F33600 (France)

* Corresponding author. E-mail : vinhola@lcts.u-bordeaux1.fr

Abstract. The Chemical Vapour Infiltration (CVI) process is used to fabricate the pyrocarbon matrices of C/C composites. This process involves complex physico-chemical phenomena such as the transport of precursor, carrier, and by-product gases in the reactor and inside a fibrous preform, heat transfer, chemical reactions (pyrolysis and deposition), and the structural evolution of the preform. It is able to provide high-quality materials because the processing conditions are rather mild with respect to the fibres; however it is expensive and sometimes difficult to optimize. This process has been the object of extensive modelling efforts, because of imperative optimization needs. The present work presents an approach suited to the exploitation of computerized microtomographs of C/C composites, which features image acquisition, computation of geometrical and transport properties, and infiltration modelling, as applied to the infiltration of needled carbon fibre fabrics. Another application to the reinforcement of carbon foams is also presented, as an example of inserting this approach in a global modelling strategy.

1. Introduction

Fibre-reinforced carbon-matrix (C/C) composites are dedicated to very high-performance and high-cost applications, mainly in the domain of aerospace technology [1], as thermal protection systems, rocket engine hot parts, or aircraft brakes, as well as plasma-facing components in Tokamak reactors [2]. Design, fabrication and characterization of this class of materials involve large efforts towards the best possible quality, in terms of mechanical and thermal performances, and resistance to physico-chemical erosion. Since the fabrication processes and the high-temperature tests are extremely expensive, there is an evident interest in increasing as much as possible the knowledge on the involved physics and chemistry, in order to produce reliable modelling approaches. One part of the knowledge on the C/C materials that has to enter the modelling approaches is a sound description of the composite morphology, which may be rather complex in some cases. This is where the use of X-ray Computed Micro-Tomography brings help, because of its exceptional capacity for the acquisition of large, accurate 3D images of the material structure.

Carbon-carbon composites are produced, among other processes, by chemical vapour infiltration (CVI): a heated fibrous preform is infiltrated by the chemical cracking of a vapour precursor of the matrix material inside the pore space of the preform [3]. The quality of materials prepared by CVI relies on processing conditions (such as vapour precursor concentration, temperature and pressure), as well as on intrinsic properties of the preform. Experimental determination of the conditions which lead to an optimal infiltration is time-consuming and expensive. That is the reason why a global modelling of CVI is of great interest to optimize the final density and homogeneity of the composites [4-9]. This modelling requires a good knowledge of geometrical characteristics and transport properties of the preform at various stages of infiltration [10], namely: the effective gas diffusivity, either in continuum or in rarefied regime, the gas permeability to viscous flow, and the heat conductivity, in the case of thermal-gradient modifications of CVI [11].

In this paper, we will try to review some CMT-based modelling efforts in these directions. The first part will address the preliminary duty of 3D image (block) acquisition, which in the case of synchrotron X-ray CMT is already an issue; the second part recalls some results on the assessment of geometrical and transport properties in C fibre preforms partly infiltrated with C matrix, and addresses infiltration modelling; and the third one presents an application case, concerning carbon foam reinforcement by pyrocarbon. Finally, some conclusive remarks and guidelines are given.

2. Image acquisition

In order to have a good representation of the C/C composite architecture, CMT scans may be performed at various scales: indeed, the diameter of a single fibre is roughly 8 μm , while the space period of the textile arrangement may span several millimetres. Fortunately, all these scales are accessible to X-ray CMT, using classical X-ray sources for the largest ones and Synchrotron Radiation X-ray CMT (XRCT) for the smallest. However, in this last case, one has not a direct access to the density distribution in the material. Indeed, the difference between the absorption coefficients of the carbon fibres, the carbon matrix, the embedding matrix that has sometimes to be used in sample preparation, and air is small and the contrast is faint. Nonetheless, the highly coherent character of the quasi-parallel, monochromatic X-ray beam from synchrotron sources allows for characterizations based on the refractive index contrasts, which are approximately 1000 times larger than the absorption contrasts [12]. Two approaches are then possible: first, the complete refraction index reconstruction, called holotomography [13], and second, the phase-contrast edge-detection mode, associated to image processing for the segmentation of the constitutive phases. These extra difficulties partly explain why there has been a large time gap between the first successful characterizations of the structure of SiC fibre cloth lay-up preforms at bundle scale (pixel size of 15.6 mm) [14,15] and the same kind of work on C/C composites.

Details on the experimental procedure have been given in [16,17]. The samples were raw and partly infiltrated C fibre preforms made of stacked satin weaves held together by stitching; they have been scanned with a 0.7 μm voxel edge size resolution, using the setup of the ESRF ID 19 beamline. Lower resolution scans (6.7 $\mu\text{m}/\text{voxel}$) were also made on the same samples, in order to connect with a maximal confidence the fibre-scale and larger scales, like the Representative Elementary Volume (REV) scale. Figure 1 displays a lower resolution image of the whole sample, the upper part of which has been scanned with higher resolution.

Even if holotomographic has been capable of yielding promising results on C/C composites [16], we present here the alternative approach, which consists in applying specific image processing steps to the tomographic reconstruction obtained with only one set of projections, with a sample-to-detector distance chosen such as Fresnel fringes are clearly visible [18,19]. This provides a strong edge-enhancement effect at any material discontinuity, which has principally been used in a qualitative way for the detection of interfaces. However, there are possibilities of extracting a full representation of the material phases through image processing techniques. In the case of C/C composites, a first algorithm has been developed for the separation of void (or resin) and solid phases, which display the strongest edge-enhancement effect [20]. It consists in a region-growing algorithm, preceded by a hysteresis step which ensures the continuity of the edge-enhancement pattern. The result of this procedure, applied to a raw fibre preform, is illustrated in Figure 2.

Later on, more elaborate techniques have been applied, in the aim of providing a full segmentation of fibres, matrix and void phases. For instance, Martin-Herrero and Germain [21] have designed and successfully tested an algorithm based on a differential profiling method to detect areas between intensity edges on every 2D cross section parallel to the reference system, which are then refined by correlating the outputs in 3D, followed by a "heavy-ball" fibre individuation procedure. Another method [22] uses directly the image gradient (and principally the edge-enhancement patterns) for the estimation of the localization of fibre axes; once the axes have been isolated, a gradient-sensitive region-growing procedure may be applied for the segmentation of the fibres first and then of the matrix. The result of this algorithm is presented in figure 3.

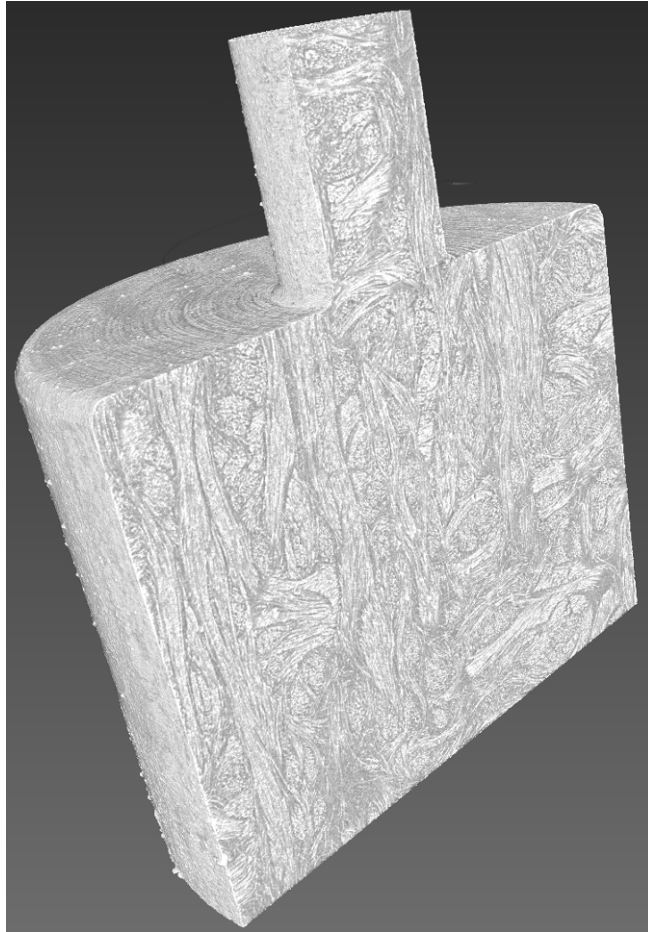


Figure 1. C/C sample for CT acquisition at 2 distinct resolutions. Sample outer diameter is 6 mm.

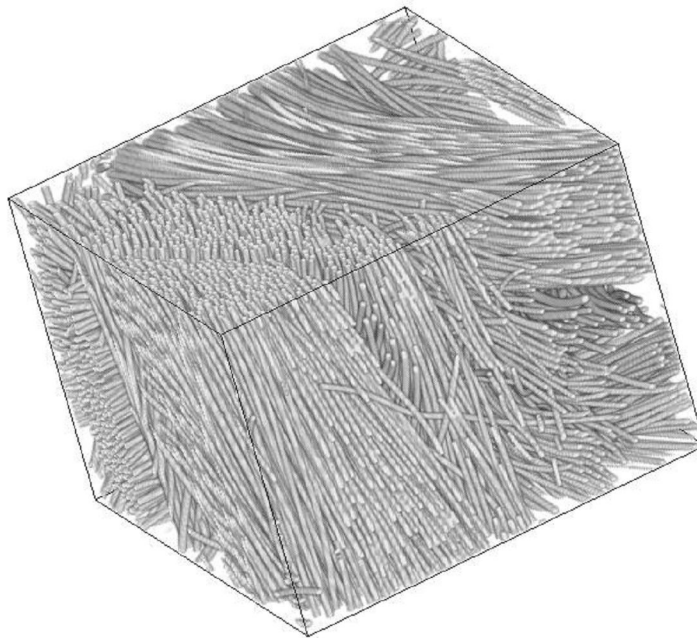


Figure 2. Segmentation of C fibres in a raw preform from an edge-detection tomographic scan.

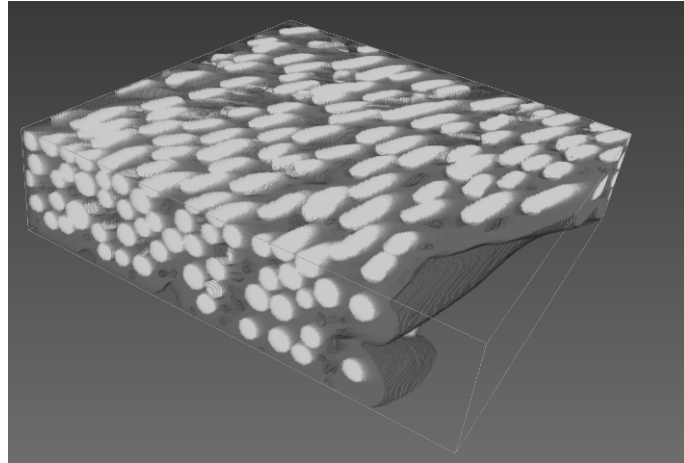


Figure 3. Segmentation of fibres and matrix in a C/C sample from an edge-detection mode

Once a proper segmentation of the solid and void phases is available, the first characterisation that can be carried out concerns the geometrical properties of the medium [17]. Pore volume measurements performed on the high-resolution scans have proved to be consistent with experimental determinations; moreover, the convergence towards an REV size has been obtained for volumes larger than 0.03 mm^3 (*i.e.* edge size superior to $\sim 0.3 \text{ mm}$). Internal surface area has been determined by a Simplified Marching Cube discretization [23,24]. The total surface area has been found coherent with the experimental values, provided the sub-micrometric roughness contribution (not accessible to this μCT experiment) is removed. Also, the pore size distribution has been evaluated and compared to experimental data from Hg intrusion curves, showing excellent agreement [25].

Characterization of the samples obtained at lesser resolution features two tasks, suited for the modelling targets: the first one is the build-up of a correspondence table between local greyscale values and pore volume fraction, which is principally a matter of data fitting, and the second one is the detection of the local orientation of the fibres. The latter operation has been performed by splitting the blocks into very small sub-volumes, thresholding them arbitrarily to 50% void space, utilizing a random-walk algorithm sensitive to the local anisotropy, and extracting the eigenvectors and eigenvalues of the pseudo-diffusion tensor resulting from the random-walk displacement covariance matrix. The largest eigenvalue indicates the direction of preferred diffusion, which is assimilated to the local fibre orientation. The method has been tested against more traditional approaches based on 2D images, and proved to account quantitatively for the volume fraction of vertical fibres [17].

3. Physico-chemical modelling for CVI based on CMT images

The necessary steps for CVI modelling are, besides the geometrical quantities, the determination of effective gas transfer properties (in continuum and rarefied regimes), of heat transfer properties, and the prediction of the porous medium evolution under infiltration.

Effective gas transport coefficients are calculated in high-resolution images with a random walk algorithm, making use of our surface triangulation scheme [23]. Indeed, there are three diffusion regimes depending on the Knudsen number Kn , which is the ratio between the mean free path of the molecules and the pore diameter : the ordinary regime ($Kn \ll 1$), the transition regime ($Kn \sim 1$), the Knudsen or rarefied regime ($Kn \gg 1$), all three of importance in CVI. The random walk performed by the molecules introduced in the void space is directly linked to the Knudsen number and it allows determining the effective diffusivity tensor \underline{D} at any value of Kn . The tortuosity tensor components η_{ij} are then calculated using the equation $\eta_{ij} = \varepsilon D_{ref} D_{ij}^{-1}$ where ε is the porosity and D_{ref} the gas diffusivity in void space. Fig. 4 is an example of the results produced by this method for Knudsen transport in transverse direction in numerous sub-samples with $100 \times 100 \times 100$ cubic voxels size [26]. The laws that have been fitted to the values computed from the CMT sub-samples are somewhat intermediate between

ideal media made of random straight cylinders: parallel to each other (1D), grouped into mats (2D), or isotropic (3D), with or without overlap between cylinders. Although most of the fibres are rather locally oriented in a parallel fashion, it appears that the 1D models are not the most suited to describe them. Indeed, the discrepancies with the 1D non-overlapping, random cylinder ideal media arises principally from the non-strict alignment between contiguous fibres, a fact which lowers considerably the percolation threshold [27].

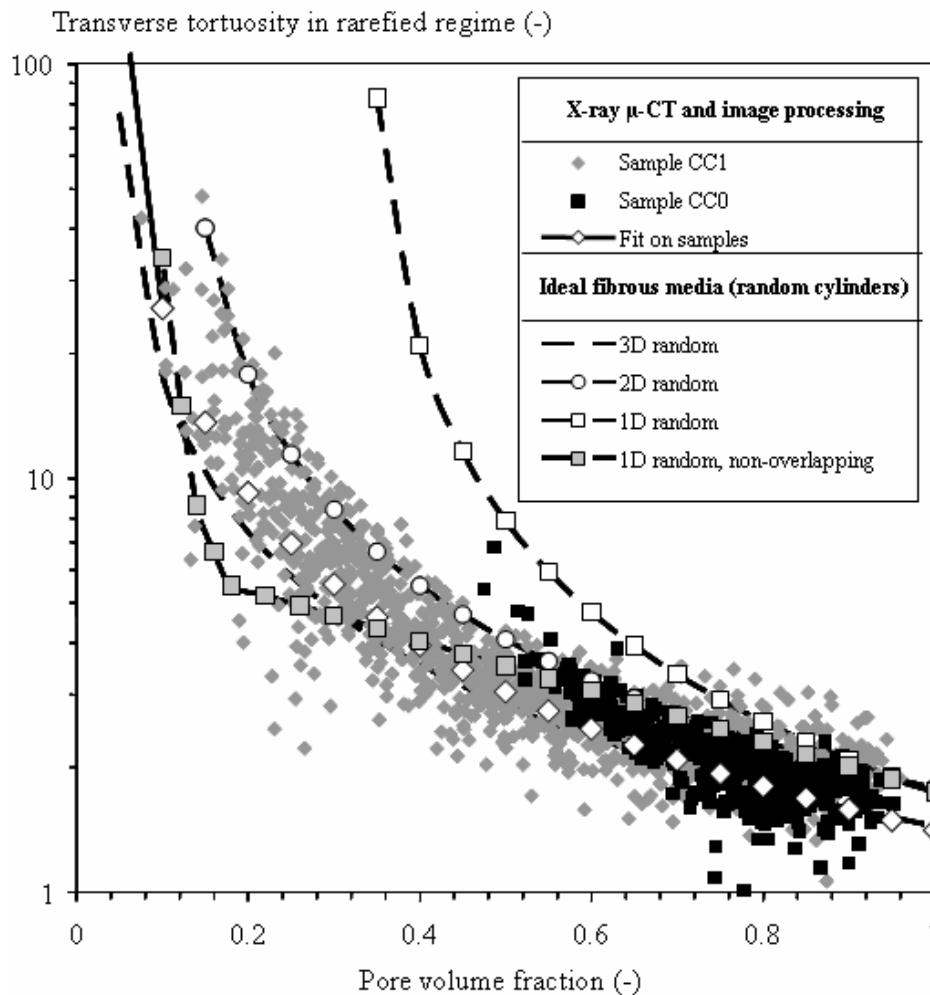


Figure 4. Tortuosity–porosity correlation plots for Knudsen transport in transverse direction. Comparison of CMT data with correlations for ideal fibrous media.

Estimates of the gas transport properties at a larger scale have been performed using a second change-of-scale strategy based on the correlation between greyscale levels and pore space, plus the computation of the local fibre orientation as mentioned earlier. A reasonable agreement has been reached with experimental determinations performed in our laboratory [26].

In the case of heat conduction, it has been possible to provide a direct comparison with experimental data. The microscopic laws have been produced through the study of ideal structures made of an isotropic fibre surrounded by an anisotropic pyrocarbon deposit (with cylindrical symmetry). Values for the individual components have been selected from experimental measurements at LCTS[28] and CEA[29], and inserted into an effective property computation code working on periodic unit cells. By varying the pyrocarbon volume fraction, taken as $(\epsilon_0 - \epsilon)$, a microscopic-scale law has been produced. Then, the second change of scale performed on low-resolution images with local orientation detection gave predictions in good agreement with direct experimental thermal measurements on the composites [30].

Finally, an adaptation of the Monte-Carlo Random-Walk algorithm has been designed for the fibre-scale modelling of chemical vapour infiltration [31]. It allows an easy handling of sticking events for the walkers, the sticking coefficient being computed from the diffusion/reaction ratio ; in case of surface growth, the surface triangulation update is fast and efficient thanks to the Simplified Marching Cube algorithm. The case of methane pyrolysis has a characteristic behaviour on the level of chemical dynamics: the first step is a slow decomposition of the relatively stable methane molecule; then, rapid reactions follow, involving a variety of radicals. If a surface is present, then deposition has to be considered as one of those fast reactions. This is best represented in the random-walk algorithm by a random introduction of the walkers in the accessible void space, the walkers representing the radical intermediates instead of the methane molecules. A closed porosity detecting routine is used to avoid unrealistic pore infiltration. Figure 5 is an example of infiltration movie obtained on a 100x100x100 cubic voxels image. Moderate values of the mean free path and sticking probabilities have been chosen. The total infiltration has been run in 6 hours 30 on a Pentium4 CPU with 3.2 GHz clock rate. Such a kind of program is able to deliver a precise evolution of the internal surface area and transport properties (diffusivities, etc ...) as a function of infiltration progress. Results are summarized as the evolution of the scaled Thiele modulus, defined as:

$$\Phi / \Phi_0 = \sqrt{\frac{\sigma_v D_0}{D \sigma_{v0}}} \quad (1)$$

This quantity collects the two most important factors determining pore accessibility, *i.e.* the internal surface area, σ_v , and the effective gas diffusivity D , as compared to their initial values. Large values of the Thiele modulus denote low “infiltrability”, that is, a low capability to receive additional amount of matrix by chemical vapour deposition.

Such an approach is a valuable tool for large-scale infiltration modelling [32], as will be illustrated in the following section.

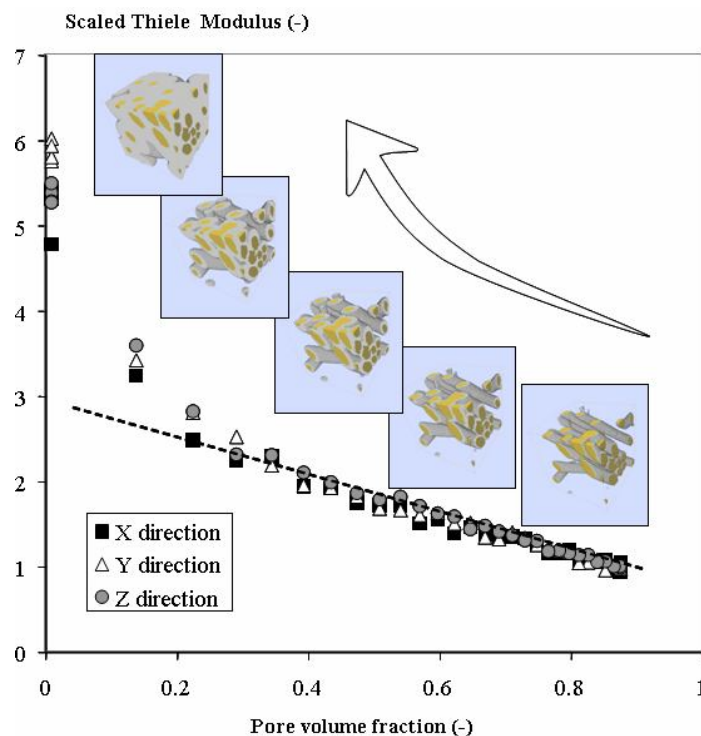


Figure 5. An example of infiltration simulation in a 100x100x100 block. Mean free path : 1 voxel (0.7 μm) ; sticking probability : 0.166. The graph is the evolution of the scaled Thiele modulus as the pore volume decreases.

4. Application to infiltration of carbon foams by pyrocarbon

Carbon foams are attractive potential materials for shock insulation in extremely high temperatures; but the mechanical properties of the as-prepared foams are too low. Chemical Vapor Infiltration (CVI) of carbon or refractory ceramics is an interesting solution to overcome this drawback.

Carbon open-cell foams [33] provide a unique opportunity to obtain a global validation of the integrated modelling approach. Indeed, their geometrical properties are rather easy to assess and model and their surface-to-volume ratio is low enough to ensure a correct infiltration, which helps in transposing results from CVD situations to CVI [34]. Here, results are presented on the deposition of pyrocarbon from pure propane in carbon foam samples with ~ 96% initial porosity, the treatment being stopped when porosity reaches ~85%. Using pure propane as a precursor, it is possible to perform deposition of three distinct kinds of laminar pyrocarbons. When increasing either the residence time or the process temperature, one obtains successively [35]: i) Granular and Columnar (GL and CL) laminar pyrocarbons, collectively denominated Rough Laminar (RL), ii) Weakly anisotropic laminar (WAL), also known as Smooth Laminar (SL), and iii) Highly Anisotropic Laminar (HAL), also known as Regenerative laminar (ReL) [36], which had long been mistaken for RL. We will restrict ourselves to the last two forms of pyrocarbon, WAL and HAL, for which the deposition rates are neatly distinct, HAL deposition being much faster. Depending on the chosen nanotexture, infiltration gradients are more or less marked in the samples.

The modelling approach [37] combines three elements, as described in Figure 6 : i) a chemical kinetic scheme which accounts correctly for the deposition of HAL and WAL depending on the reactor processing parameters, ii) the CMT-based infiltration modelling as presented in the preceding section, and iii) a reactor-scale solver collecting the results of the first two elements as input. Figure 7 gives a comparison between the experimentally determined deposit thicknesses and the same quantity, as computed by the modelling approach, showing very reasonable agreement between both.

The conditions were such that there is a marked difference between WAL and HAL pyC infiltration, in terms of final gradients. Indeed, WAL pyC deposition is a rather slow process, 5 to 10 times slower than HAL pyC deposition. In this case, the consumption of direct precursors of the deposit is balanced by diffusion of the primary source and its transformation into the direct precursor: this leads to extremely low gradients. Actually, some conditions have been given in which inside-out infiltration occurs [38,39]. Conversely, WAL pyC direct precursors are consumed too quickly to be renewed by diffusion and homogeneous reactions, and the final consequence is the build-up of a marked infiltration gradient.

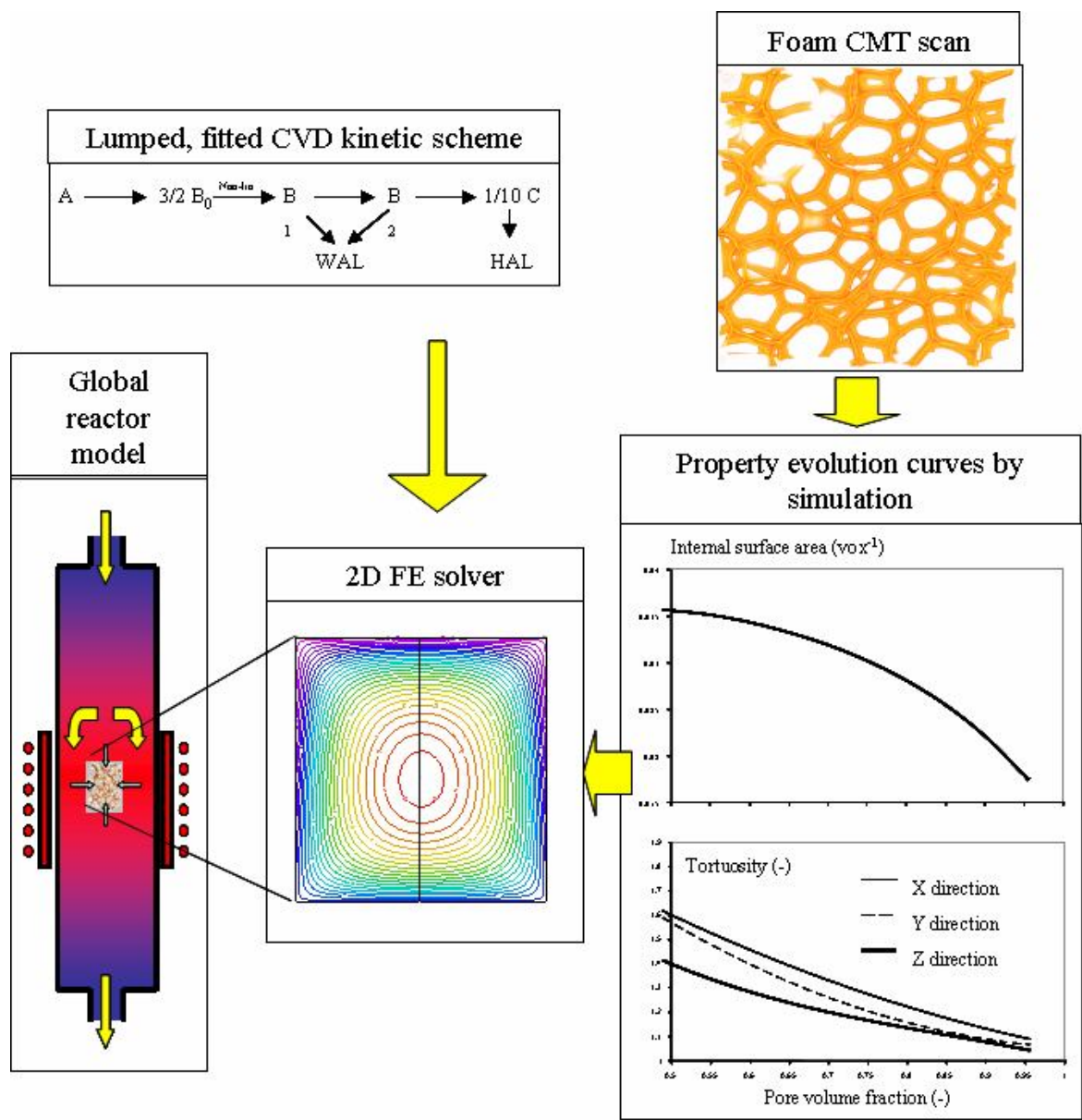


Figure 6. Presentation of the global modelling strategy as applied to carbon foam reinforcement by pyrocarbon CVD.

4. Conclusion

This paper has summarized some efforts made in the characterization of C/C composites as a tool for modelling their preparation by chemical vapour infiltration. High-resolution X-ray tomographic imaging has proved extremely valuable, because of its excellent space resolution. A two-scale approach has been developed to account for the structure of the composite material. The studies have involved image processing and pattern recognition, morphological analysis, and direct numerical simulation of reaction/diffusion systems with moving boundaries. Results show that the assessment of geometrical and transport properties throughout the material evolution is possible on the basis of CMT images; the incorporation of the structure-property relationships in large-scale models of processes and/or degradation tests is indeed of large value and is still currently undergoing. An application to the reinforcement of carbon foams by pyrocarbon CVD, including the complex homogeneous chemistry of propane decomposition, is presented as a validation.

Further directions are, among others, the development of more convivial image acquisition and processing cycles, the extension of the computational procedures to larger datasets, and the introduction of more complex heterogeneous reaction kinetic schemes.

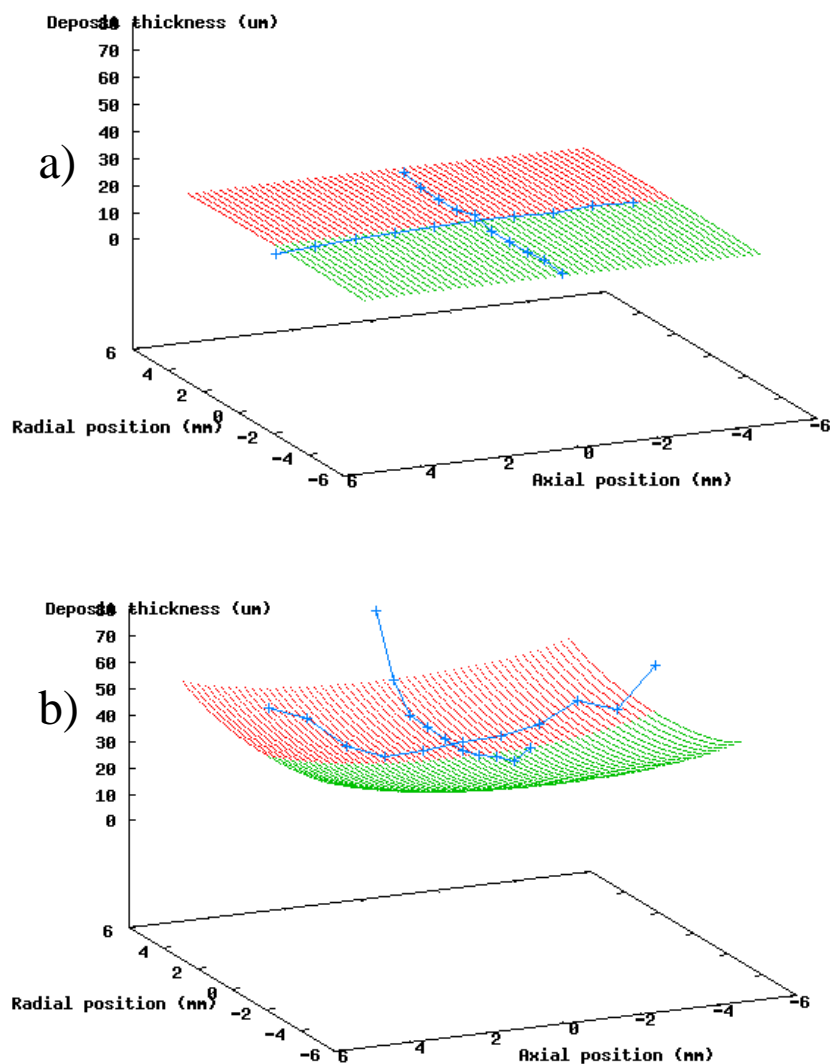


Figure 7. Comparison of computed and measured deposit thicknesses throughout foams in conditions of (a) WAL pyC and (b) HAL pyC deposition.

References

- [1] G. Savage, *Carbon/Carbon composites*, Chapman & Hall, London, 1993.
- [2] H.C. Mantz, D.A. Bowers, F.R. Williams, M.A. Witten, in *Proceedings of the IEEE 13th Symposium on Fusion Engineering* vol. 2, IEEE-89CH2820-9, 1990, 947.
- [3] R. Naslain, F. Langlais, *High Temp. Sci.* **27** (1990) 221.
- [4] T. L. Starr, A. W. Smith, *Mat. Res. Soc. Symp. Proc.* **250** (1992) 207.
- [5] P. McAllister, E. E. Wolf, *AIChE J.*, **39** (1993) 1196.
- [6] G. L. Vignoles, C. Descamps, N. Reuge, *J. Phys. IV France* **10** (2000) Pr2-9.
- [7] N. Reuge, G. L. Vignoles, *J. Mater. Proc. Technol* **166** (2005) 15.
- [8] D. Leutard, G. L. Vignoles, F. Lamouroux, B. Bernard, *J. Mater. Synth. and Proc.* **9** (2002) 259.
- [9] I. Golecki, *Mater. Sci. Eng.* **R20** (1997) 37.
- [10] J. Y. Ofori, S. V. Sotirchos, *J. Electrochem. Soc.* **143** (1996) 1962.
- [11] G.L. Vignoles, J.-M. Goyh n che, P. S bastian, J.-R. Puiggali, J.-F. Lines, J. Lachaud, P. Delha s, M. Trinqu coste, *Chem. Eng. Sci.* **61** (2006) 5336.

- [12] P. Cloetens, W. Ludwig, J. P. Guigay, J. Baruchel, M. Schlenker, D. Van Dyck, in : *X-ray tomography in material science*, J. Baruchel, J.-Y. Buffière, E. Maire, P. Merle, G. Peix, Eds., Hermès, Paris, 2000, p. 30.
- [13] P. Cloetens, W. Ludwig, J. Baruchel, D. Van Dyck, J. Van Landuyt, J. P. Guigay, M. Schlenker, *Appl. Phys. Lett.* **75** (1999) 2912.
- [14] J. H. Kinney, T. M. Breunig, T. L. Starr, D. Haupt, M. C. Nichols, S. R. Stock, M. D. Butts, R. A. Saroyan, *Science* **260** (1993) 789.
- [15] S-B. Lee, S. R. Stock, M. D. Butts, T. L. Starr, T. M. Breunig, J. H. Kinney, *J. Mater. Res.* **13** (1998) 1209.
- [16] O. Coindreau, P. Cloetens, G. L. Vignoles, *Nucl. Instr. and Meth. in Phys. Res. B* **200** (2003) 295.
- [17] O. Coindreau, G. L. Vignoles, *J. Mater. Res.* **20** (2005) 2328.
- [18] M. Ando, S. Hosoya, in *Proc. 6th Intern. Conf. On X-ray Optics and Microanalysis* G. Shinoda, K. Kohra, T. Ichinokawa, Eds. Univ. of Tokyo Press, Tokyo, 1972, p. 63.
- [19] P. Cloetens, M. Pateyron-Salomé, J.-Y. Buffière, G. Peix, J. Baruchel, F. Peyrin, M. Schlenker, *J. Appl. Phys.* **81** (1997) 5878.
- [20] G. L. Vignoles, *Carbon* **39** (2001) 167.
- [21] J. Martín-Herrero, C. Germain, *Carbon* **45** (2007) 1242.
- [22] C. Mulat, M. Donias, P. Baylou, G. L. Vignoles, C. Germain, *J. Electronic Imaging* **17** (2008) 0311081.
- [23] G. L. Vignoles, *J. Phys. IV France* **C5** (1995) 159.
- [24] M. Donias, G. L. Vignoles, C. Mulat, C. Germain, submitted to *IEEE Trans. on Visualization & Computer Graphics*, 2009.
- [25] O. Coindreau, G. L. Vignoles, J.-M. Goyhénèche, in *Advances in Ceramic-Matrix Composites XI*, N. P. Bansal, J. P. Singh and W. M. Kriven, Eds. *Ceram. Trans.* **175** (2005), Wiley, New York, p.77.
- [26] G. L. Vignoles, O. Coindreau, A. Ahmadi, D. Bernard, *J. Mater. Res.* **22** (2007) 1537.
- [27] O. Coindreau, G. L. Vignoles, in *Advanced Materials Forum II* (Eds.: R. Martins, E. Fortunato, I. Ferreira and C. Dias) *Mater. Sci. Forum* **455-456** (2004) *Trans. Tech. Publications*, Zurich, p. 751.
- [28] C. Sauder, PhD dissertation, Université Bordeaux 1, France (2001).
- [29] J. Jumel, F. Lepoutre, J-P. Roger, G. Neuer, M. Cataldi, F. Enguehardt, *Rev. Sci. Instrum.* **74** (2003) 537.
- [30] D. Demange, J. C. Laizet, Technical Report RT 1/03519 DMSC, ONERA, Châtillon, France (2000).
- [31] C. Mulat, PhD Thesis, University Bordeaux 1, France (2008).
- [32] G. L. Vignoles, in *Advanced Fibrous Inorganic Composites V*, P. Vicenzini, Ed., *Adv. Sci. Technol.* **50** (2006), *Trans Tech Publications*, Zürich, p. 97.
- [33] S. Delettrez, G. Chollon and F. Langlais, "Carbon open-cell foams: CVD processing and characterization" in *Proc. Carbon 2008*, Nagano, Japan (June 2008)
- [34] G. L. Vignoles, F. Langlais, C. Descamps, A. Mouchon, H. Le Poche, N. Bertrand and N. Reuge, *Surf. Coat. Technol.* **188-189** (2004) 241-249.
- [35] J.-M. Vallerot, X. Bourrat, A. Mouchon and G. Chollon, *Carbon* **44** (2006) 1833
- [36] X. Bourrat, A. Fillion, R. Naslain, G. Chollon and M. Brendlé, *Carbon* **40** (2002) 2931
- [37] G. L. Vignoles, C. Gaborieau, S. Delettrez, G. Chollon, F. Langlais, *Surf. Coat. Technol.* **203** (2008) 510-515.
- [38] S. Middleman, *J. Mater. Res* **4** (1989) 1515.
- [39] W. G. Zhang, and K.J. Hüttinger, *ECS Proceedings PV* **2003-08** (2003) 549